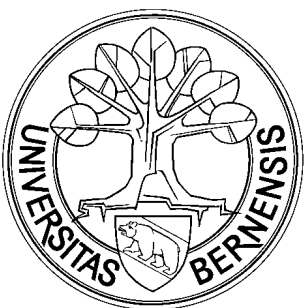

JEM/SMILES AOPT EM, Part 4

Measurements before and after SLO

Integration

Axel Murk



Research Report No. 2003-03
May 2003

Institute of Applied Physics

Dept. of Microwave Physics

Sidlerstr. 5
CH-3012 Bern
Switzerland

Tel. : +41 31 631 89 11
Fax : +41 31 631 37 65
E-mail : iapemail@iap.unibe.ch

Contents

1	Introduction	2
2	Bandpass Characteristic	3
2.1	TRN Port after FSP Tuning and SMI Activation	3
2.2	CST Port after FSP Tuning with SLO Cleanup Grid	5
2.3	Bandpass Characteristic at different Temperatures	11
2.4	Bandpass Characteristic with double RG1	15
3	SLO Integration	18
3.1	SLO Coupling	18
3.2	SLO Balance	18
4	Internal Reflections with SMI and SLO	20
5	Conclusions	30

1 Introduction

Part 4 of the AOPT EM test report documents measurements of the bandpass characteristic and internal reflections before and after SLO integration. The purpose of these measurements was to complete the tests after FSP tuning and SMI integration which were missing in Part 2 (bandpass of the CST port, different input polarizations at the TRN port), to verify the performance of the SMI and to determine the SLO coupling and balance with and without the new SLO cleanup grid.

The bandpass measurements were repeated at different AOPT temperatures to investigate thermal effects. After SLO integration a second vibration run of AOPT and SLO together proved that the SLO was not affected by the vibration levels inside of the AOPT.

The measurements with activated SMI have shown that the cross-polar leakage of RG1 has a noticeable influence on the bandpass characteristic of the TRN path. For that reason RG1 was replaced with a new double wound grid. The only measurements with the new grid in this report are the bandpass measurements at different temperatures in section 2.1.

During the measurements in this report the AOPT was in the following condition:

- Same FSP tuning as in Part 2
- SMI grid activated
- SLO mass dummy replaced by TK-RAM or SLO-EM
- SLO cleanup grid inserted after AOPT/SLO vibration
- RG1 replaced by a double wound grid (section 2.4 only)

Changes in the test setup:

- A new diode in the harmonic mixer resulted in an increased dynamic range.
- The diameter of beam transfer aperture in the COPT simulator was enlarged from 25 mm to 50 mm (similar to the AOPT) because previous S11 measurements indicated reflections from the corresponding distance.

2 Bandpass Characteristic

2.1 TRN Port after FSP Tuning and SMI Activation

First bandpass measurements after FSP tuning were given already in Part 2, but only for the TRN path and for one input polarization.

Together with the tuning of the FSP filter also the SMI grid was activated. For that reason 50% of the signal from the linear polarized source entering through the TRN BBH is now always cross-polar to RG1. By changing the polarization of the source only the phase difference between the co- and the cross-polar signal on RG1 changes. With an ideal polarizer this would not affect the bandpass characteristic of the AOPT, but with the cross-polar leakage of RG1 it leads to a shift of the rejection minima depending on the source polarization (Fig. 1).

A very similar behavior is predicted by model calculations when not only the non-ideal characteristics of the FSP grids, but also the cross-polar leakage of RG1 is taken into account. The leakage of RG1, however, must be four times larger than that of a perfect grid with a regular $25\text{ }\mu\text{m}$ wire spacing to explain the measurement results (Fig. 2 and 3). This is consistent with the results of a more detailed grid model which also includes small irregularities of the grid spacing¹.

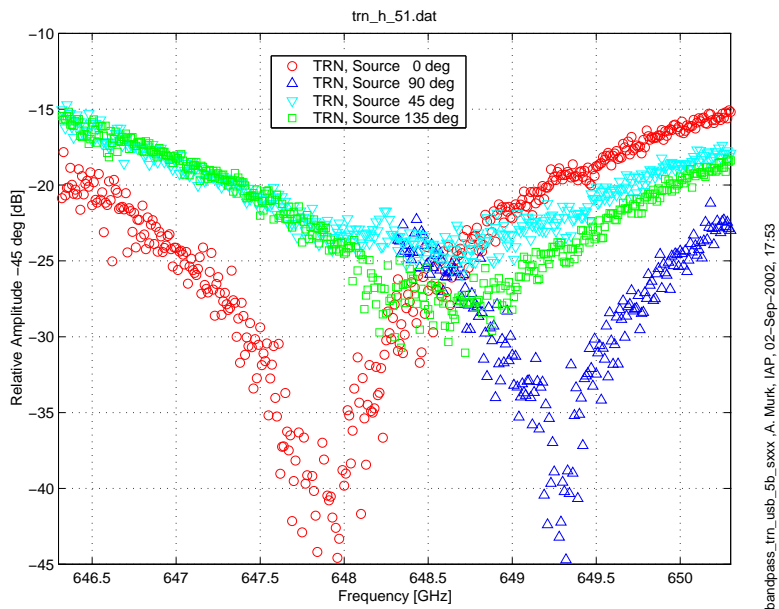


Figure 1: Measured TRN USB bandpass after FSP tuning and SMI activation for different source polarizations.

¹T. Manabe and A. Murk, *Transmission and reflection characteristics of slightly irregular wire-grids with finite conductivity for arbitrary angles of incidence and grid rotation*, Technical Report of IEICE Japan, AP2002-133, Jan. 23-24, 2003. (in Japanese).

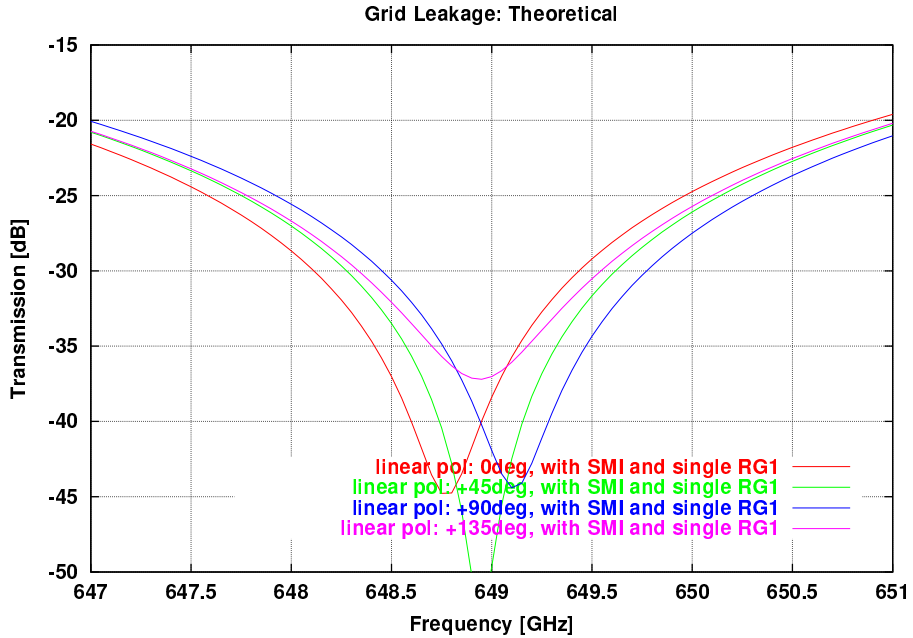


Figure 2: Theoretically calculated band-rejection characteristics for linear polarization incidence of the TRN path with SMI activated. The cross-polar leakage of RG1 was calculated for a regular grid with $10\mu\text{m}$ wires and $25\mu\text{m}$ spacing.

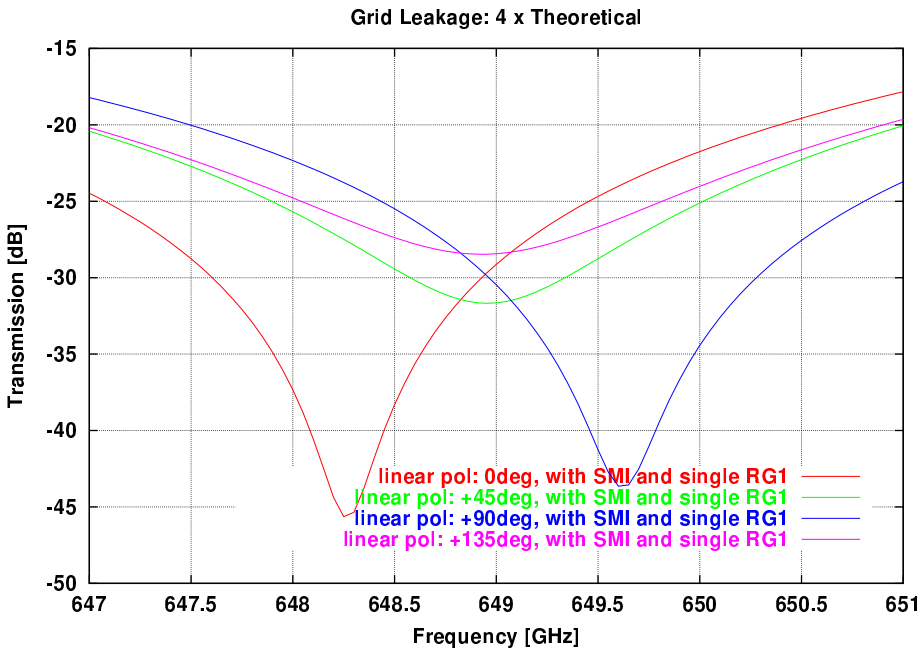


Figure 3: Same as Fig. 2, except that the amplitudes of cross-polar leakage of RG1 are assumed to be 4 times as large as the theoretically estimated values of the regular grid.

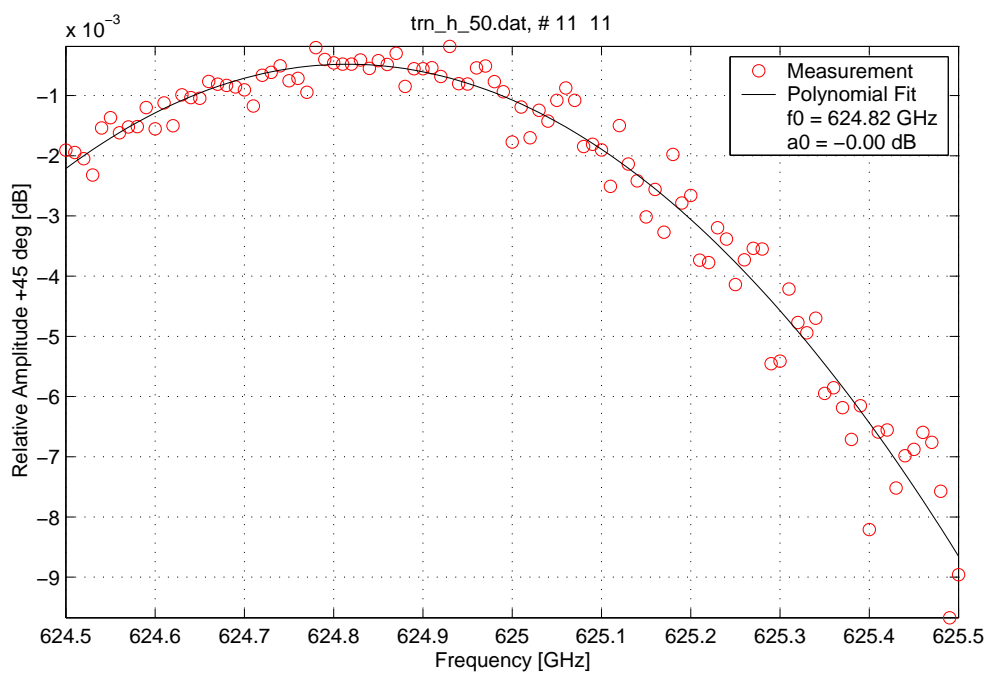
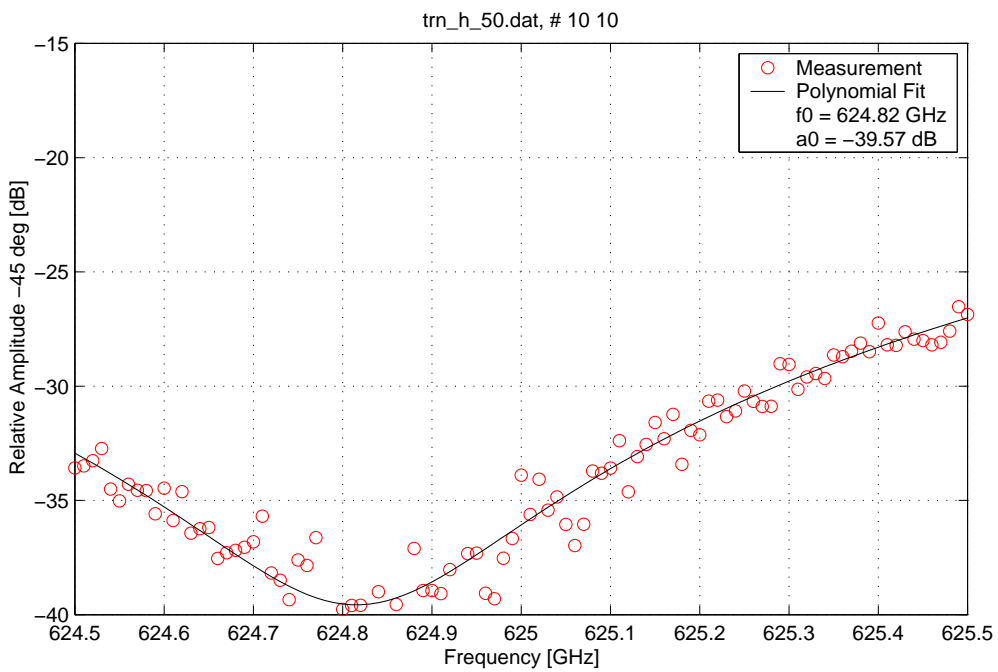
2.2 CST Port after FSP Tuning with SLO Cleanup Grid

In the original AOPT design a certain amount of cross-polar leakage was always present in the CST/SLO path caused by the polarization difference between RG1 and LG1. The results for the CST path in this configuration after FSP tuning are given in Fig. 4, 5 and 6.

As explained in section 3 the SLO balance can only be achieved with an additional cleanup grid between LG1 and RG1 which removes the cross-polar signal before RG1. Fig. 7, 8 and 9 show the CST bandpass characteristic after the integration of this grid. The results of both measurements series are summarized in Table 1.

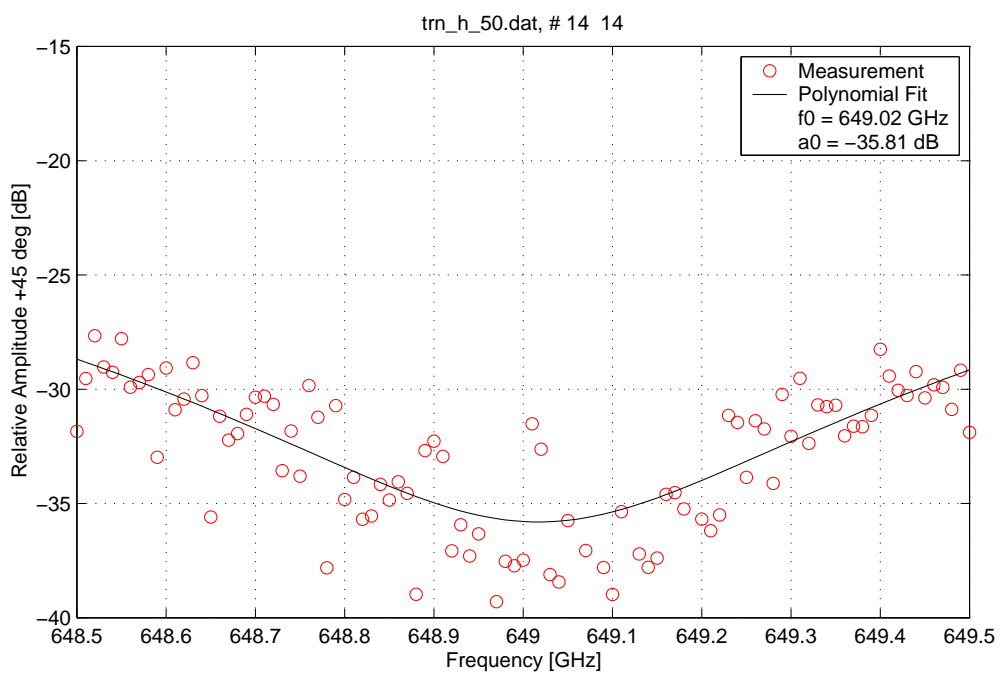
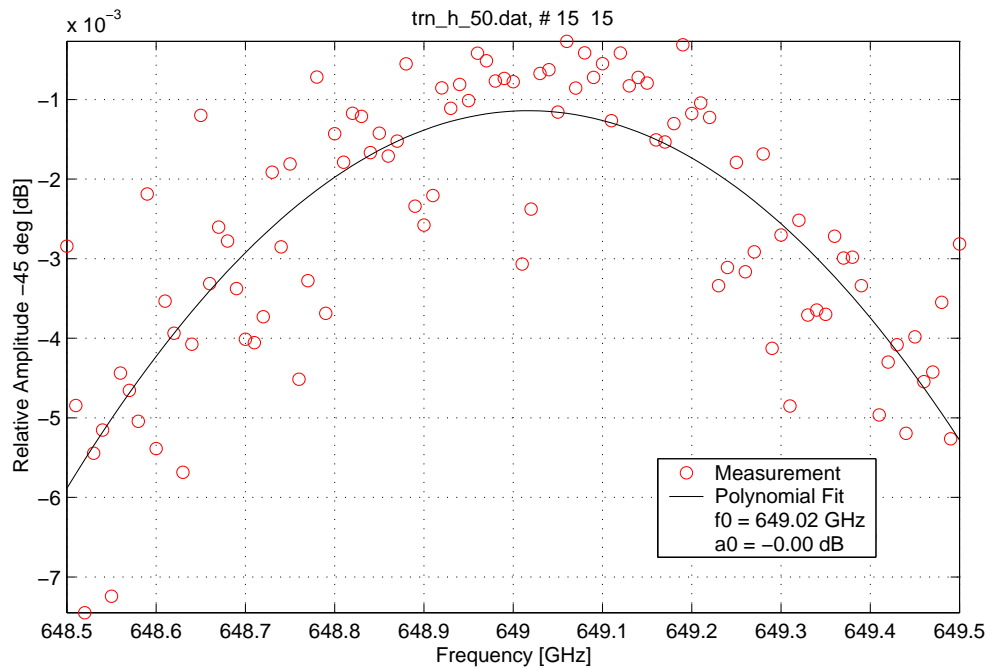
	without cleanup grid	with cleanup grid
LSB	624.82 GHz	624.41 GHz
-3dB	637.29 GHz	636.76 GHz
USB	649.02 GHz	648.51 GHz

Table 1: Rejection frequencies and cross-over frequency with and without CST cleanup grid.



bandpass_cst_h_ls5_A_Murk_IAP, 03-Sep-2002, 15:28

Figure 4: CST LSB bandpass without cleanup grid.



bandpass_cst_h_usb_5 ,A. Murk, IAP, 03-Sep-2002, 15:28

Figure 5: CST USB bandpass without cleanup grid.

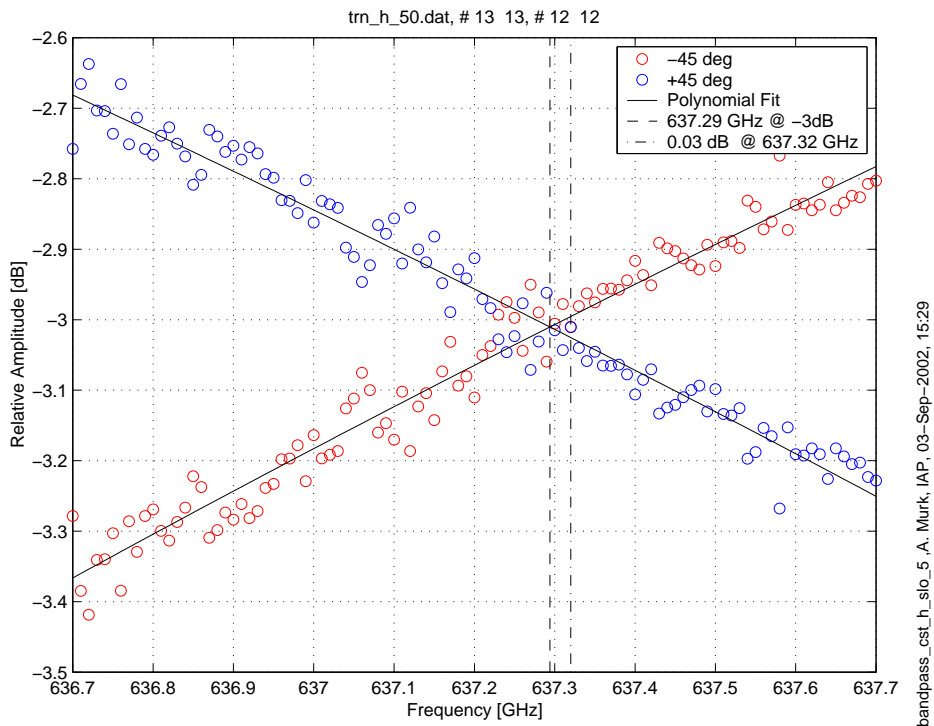


Figure 6: CST SLO bandpass without cleanup grid.

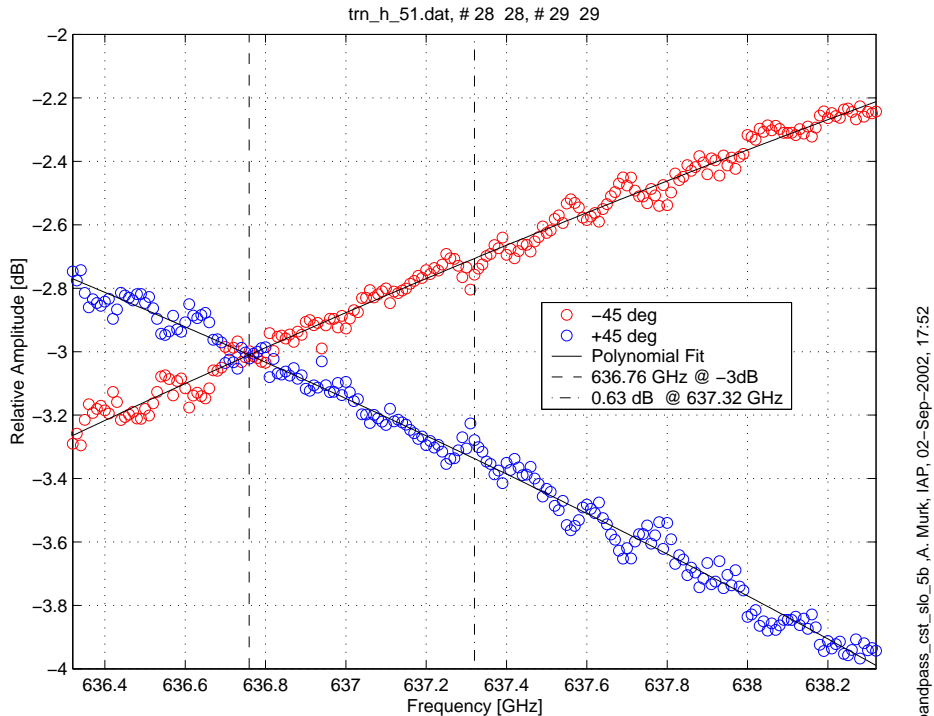


Figure 7: CST SLO bandpass with cleanup grid.

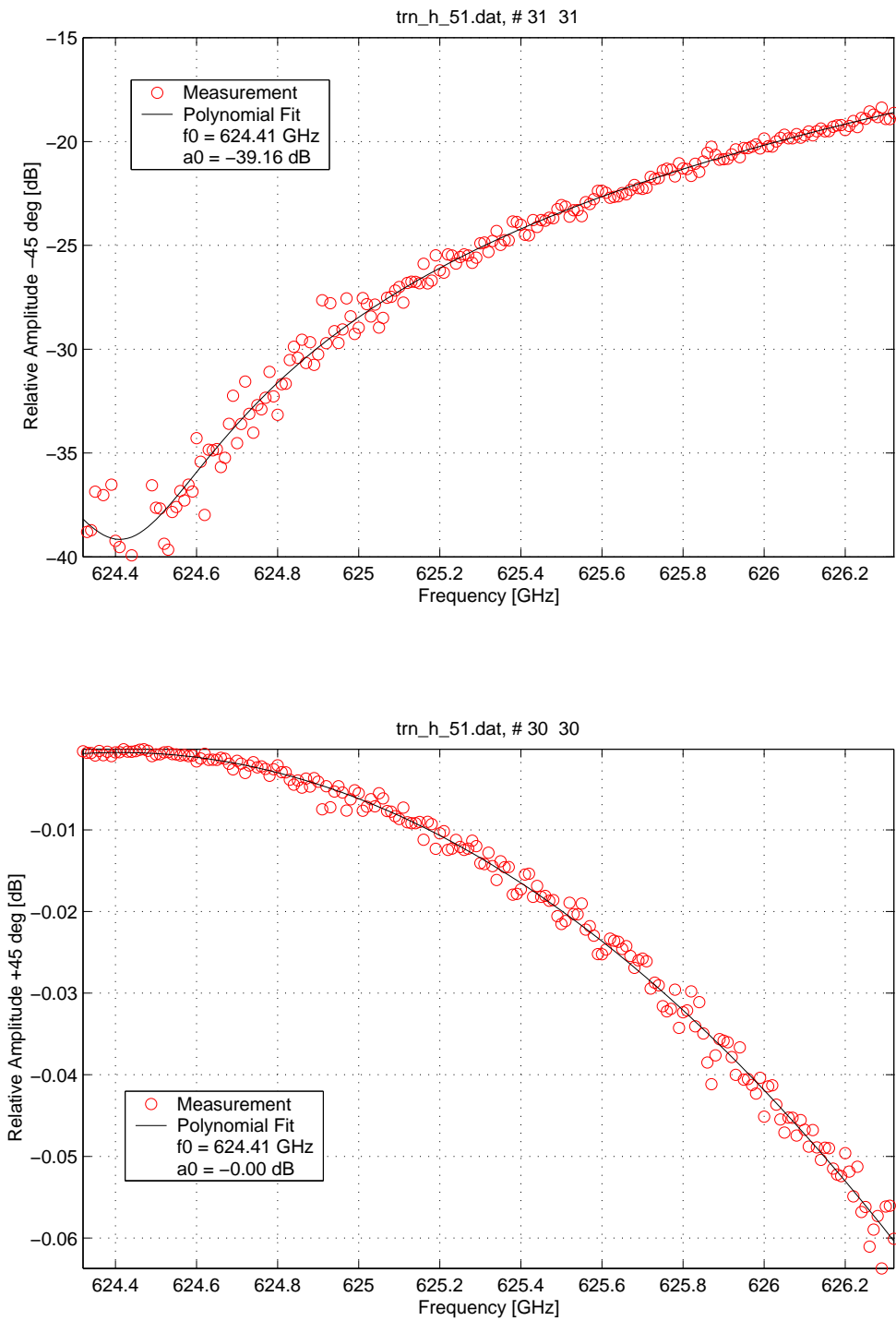


Figure 8: CST LSB bandpass with cleanup grid.

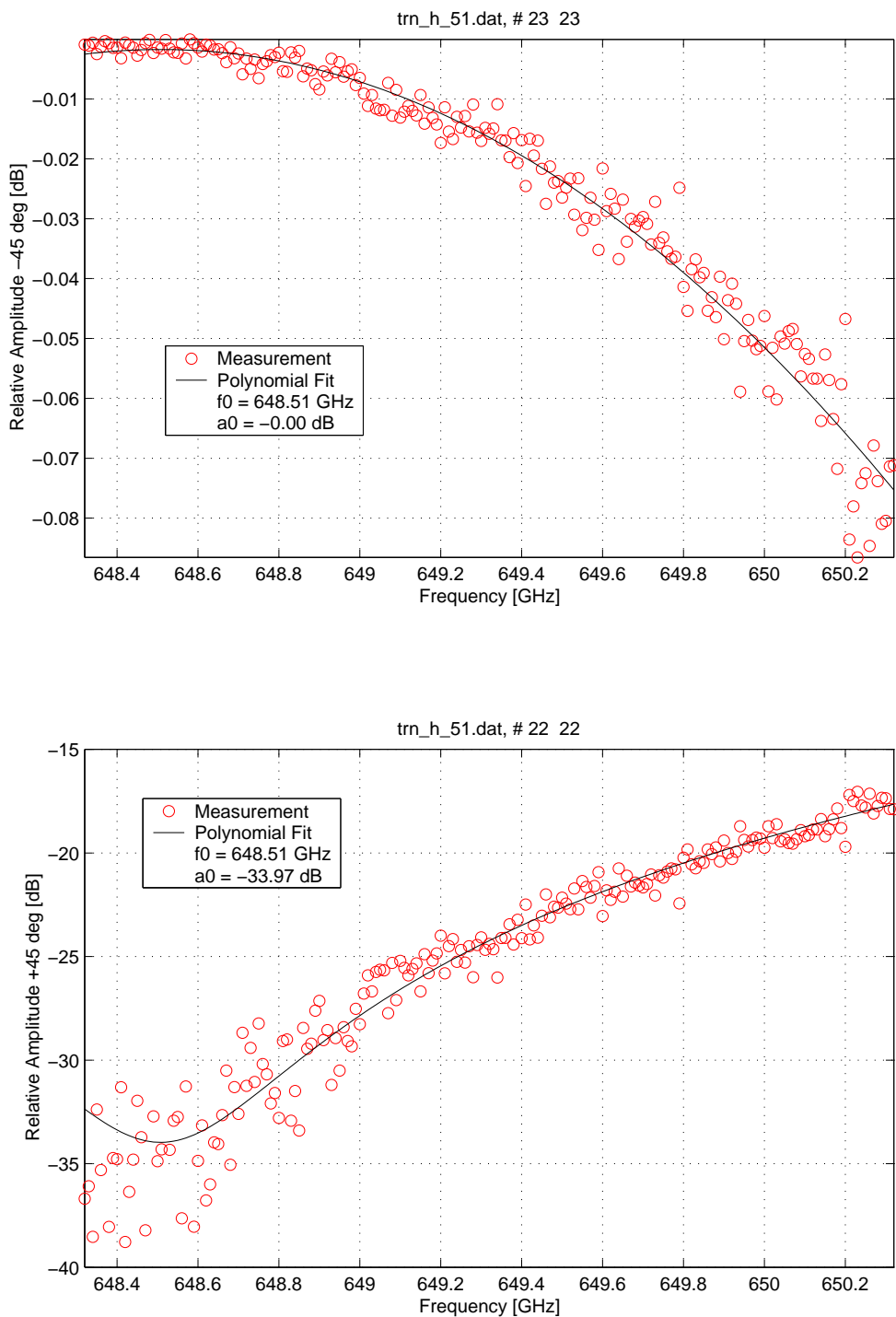


Figure 9: CST USB bandpass with cleanup grid.

2.3 Bandpass Characteristic at different Temperatures

To measure the bandpass characteristic at 40°C the AOPT and COPT simulator were heated by pumping a thermally stabilized fluid through the test fixture. With basic thermal isolation of the AOPT and a warmup time of 2 hours temperature gradients were measured to be below 2K. A first series of such measurements was done in the CST path after the integration of the additional SLO cleanup grid. The results of Fig. 10 to 12 are summarized in Table 2.

	f_0 [GHz] T=22°C	f_0 [GHz] T=40°C	Δf [MHz] 22°C → 40°C
LSB	624.41	624.72	310
-3dB	636.76	637.19	430
USB	648.51	648.98	470

Table 2: Rejection frequencies and cross-over frequency of the CST path at different temperatures.

All frequencies in this table are below their design values of 625.32, 637.32 and 649.32 GHz. These measurements, however, were all made in air, whereas the AOPT has to be tuned for operation in vacuum. Under laboratory conditions the difference between the refractive index of air and vacuum is approximately 300 ppm, which leads to an increase of the optical path difference in the FSPs. For that reason the rejection frequencies of the AOPT will increase by a similar amount (195 MHz @ 650 GHz) when the air is removed.

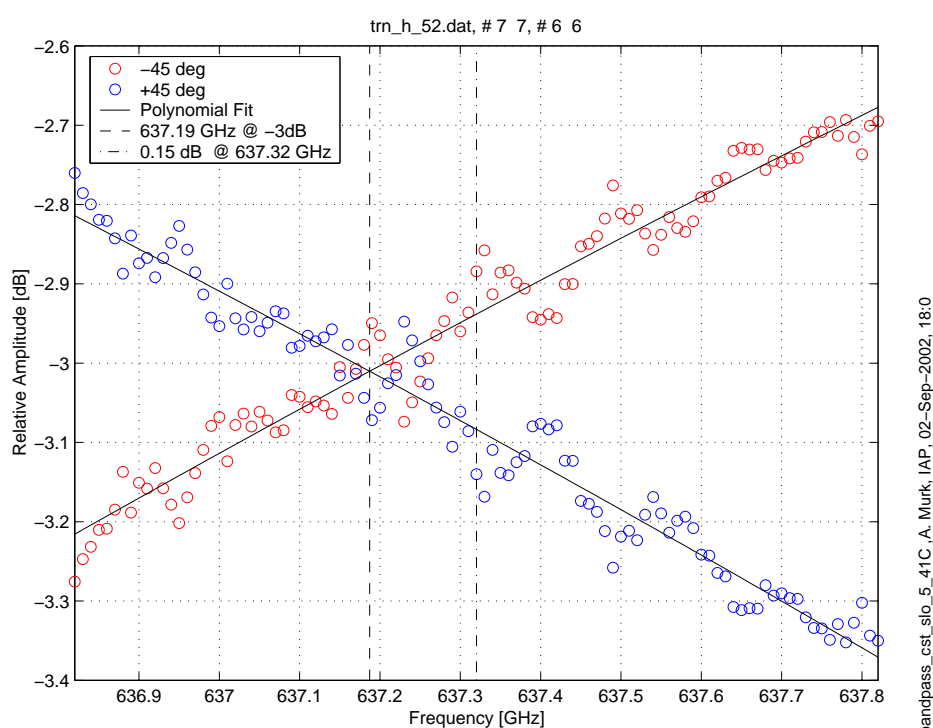
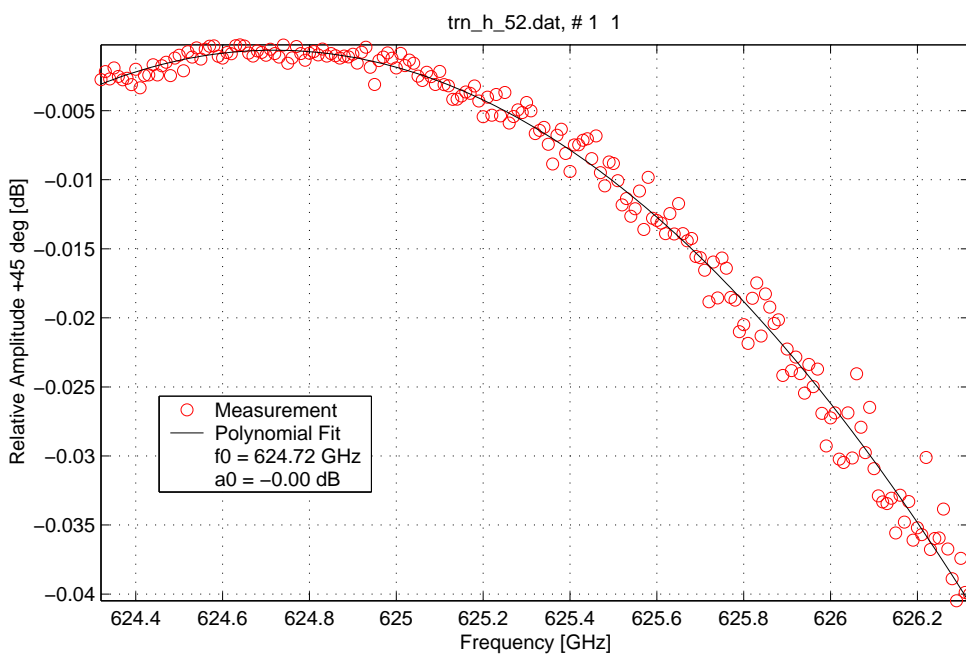
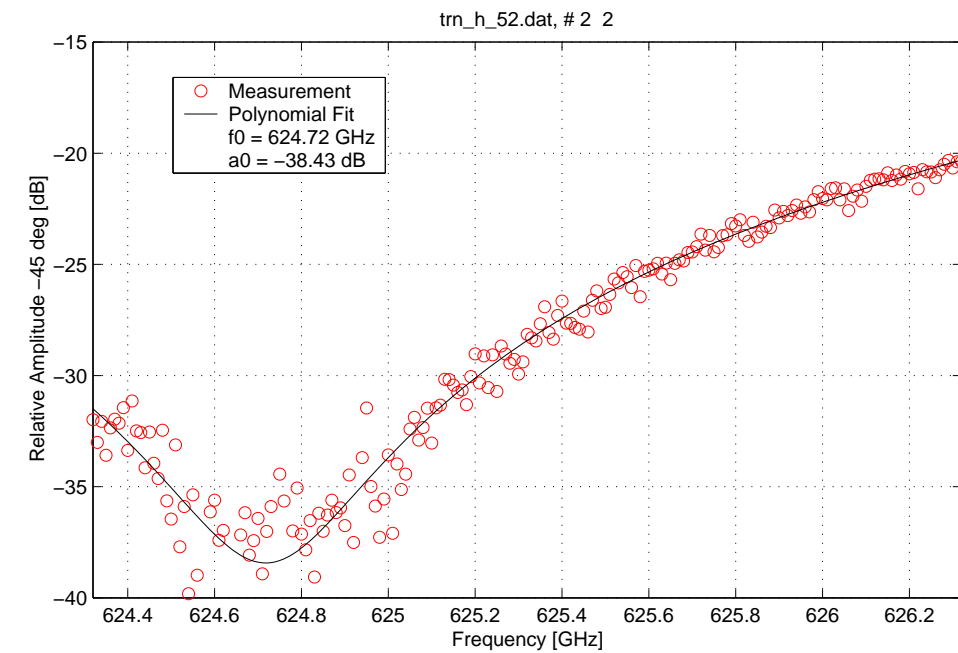


Figure 10: CST SLO bandpass with cleanup grid at 40°C.



bandpass_cst_lsb_5_41C ,A. Murk, IAP, 02-Sep-2002, 18:0

Figure 11: CST LSB bandpass with cleanup grid at 40°C.

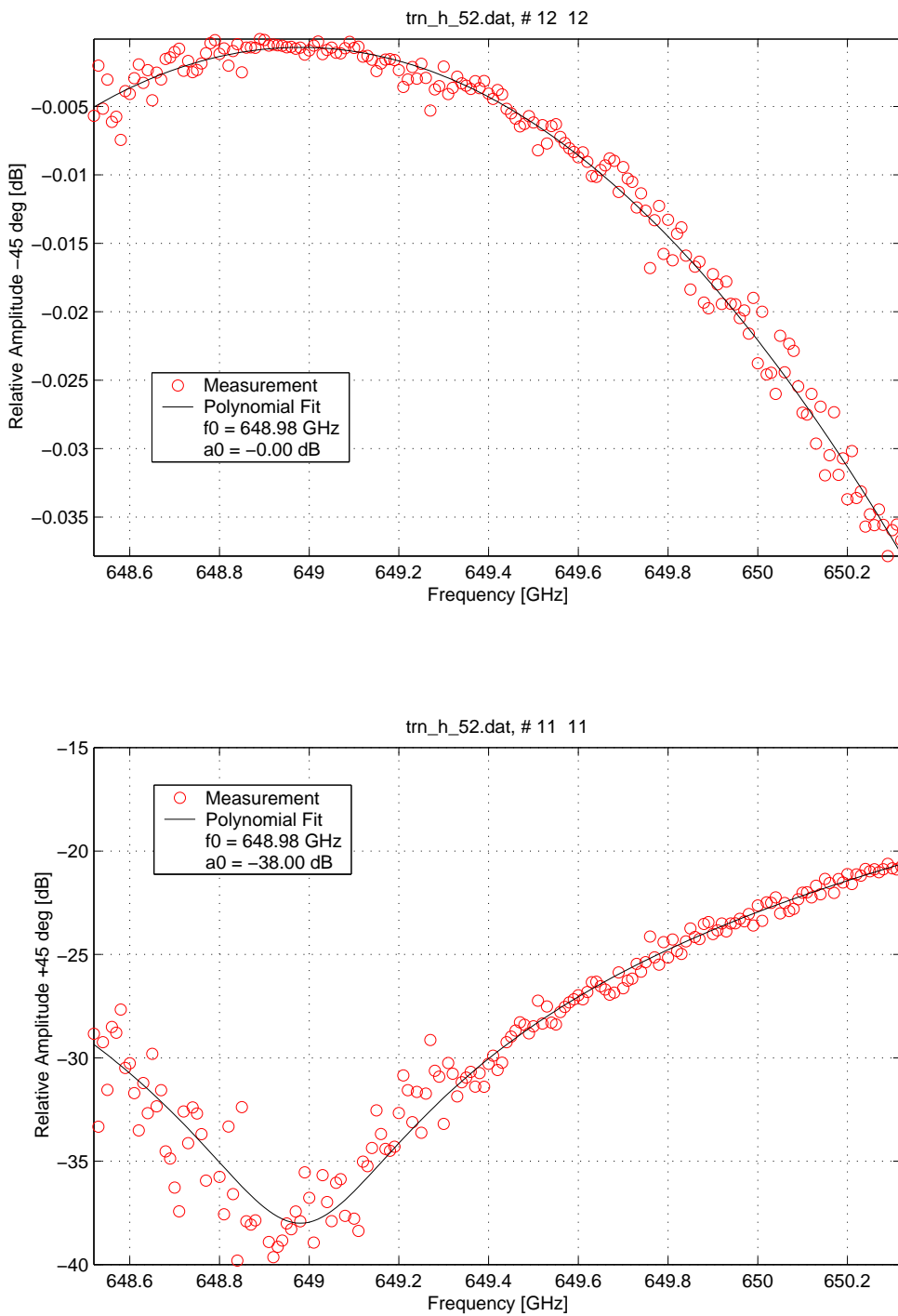


Figure 12: CST USB bandpass with cleanup grid at 40°C.

2.4 Bandpass Characteristic with double RG1

In section 2.1 it was shown that the cross-polar leakage of RG1 leads to a polarization dependent frequency response in the TRN path, especially since the performance of RG1 seems to be worse than that of a regular wire grid. For that reason RG1 was replaced by a double-wound wire grid.

To verify the unexpected large temperature dependence of the rejection frequencies in section 2.3 the bandpass measurements were repeated in the TRN and CST path at different temperatures after integration of the double RG1. The measurements in Fig. 14 and 13 confirm that the double grid leads to an almost identical bandpass characteristic of the TRN and the CST path which is independent from the input polarization.

There is still a significant temperature effect on the rejection frequencies, but slightly less than in the previous section. The values in Tab. 3 indicate a linear frequency shift of 12 MHz/ $^{\circ}$ C in both sidebands over a temperature range from 10 $^{\circ}$ C to 40 $^{\circ}$ C. Fig. 15 shows the difference between these measurements and the nominal vacuum values of 625.32 GHz and 649.32 GHz for the LSB and the USB, respectively.

Table 3: Rejection frequencies at different temperatures with double RG1:

	f_0 [GHz] $T=10^{\circ}\text{C}$	f_0 [GHz] $T=20^{\circ}\text{C}$	f_0 [GHz] $T=30^{\circ}\text{C}$	f_0 [GHz] $T=40^{\circ}\text{C}$	Δf [MHz] $20^{\circ}\text{C} \rightarrow 40^{\circ}\text{C}$
CST LSB		624.42		624.67	+250
TRN LSB	624.29	624.39	624.55	624.64	+250
CST USB		648.68		648.94	+260
TRN USB		648.70		648.94	+240

The frequency shift with the temperature is too big to be caused by the thermal expansion of the Invar FSPs. A possible explanation is the thinning of the FSP mirror from the differential expansion between Al and Invar. This effect should lead to a frequency shift into the same direction, but only about half as far as in the observations.

According to the AOPT specifications the image band rejection must be better -15 dB over the full bandwidth of USB and LSB for temperatures between +10 $^{\circ}$ C and +40 $^{\circ}$ C. The observed temperature shift leads to an improvement of the bandpass characteristic at the upper end of the temperature scale. At +10 $^{\circ}$ C the rejection frequency in the LSB is about 1 GHz below the design value, and 2 GHz below the edge of that band, but Fig. 16 shows that this is still compliant with the -15 dB requirement. In addition, operation in vacuum will also improve the image rejection with the current FSP tuning.

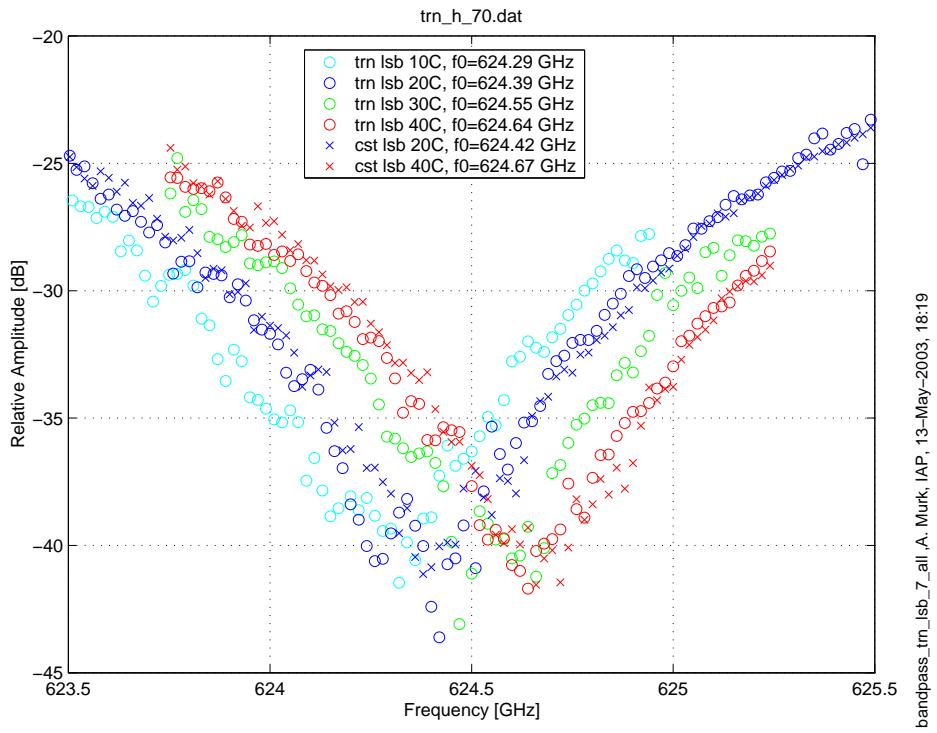


Figure 13: LSB bandpass of the CST and TRN path at different temperatures.

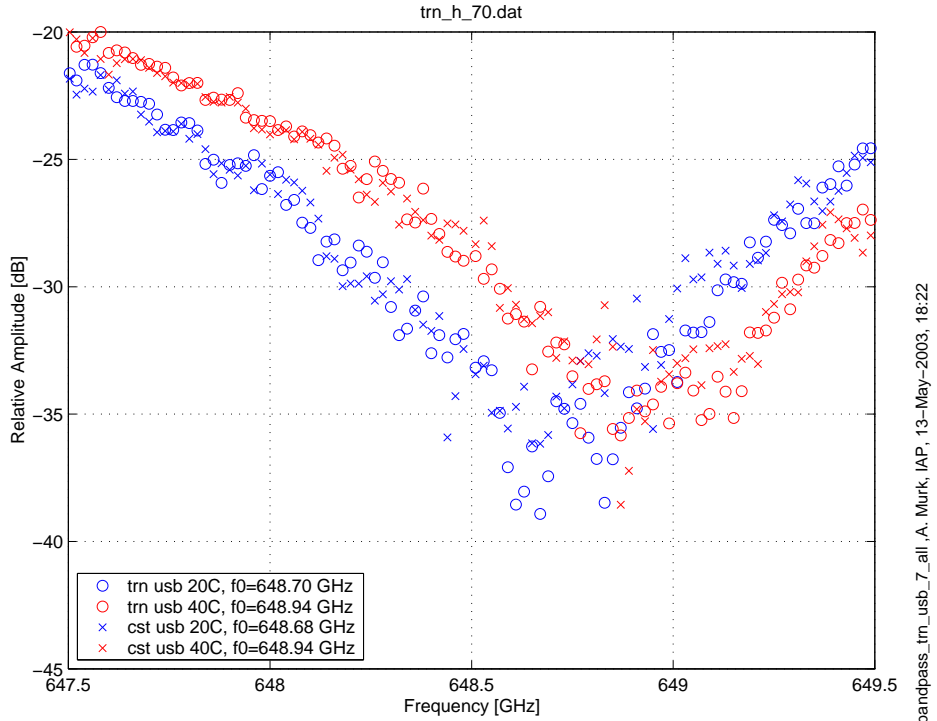


Figure 14: USB bandpass of the CST and TRN path at different temperatures.

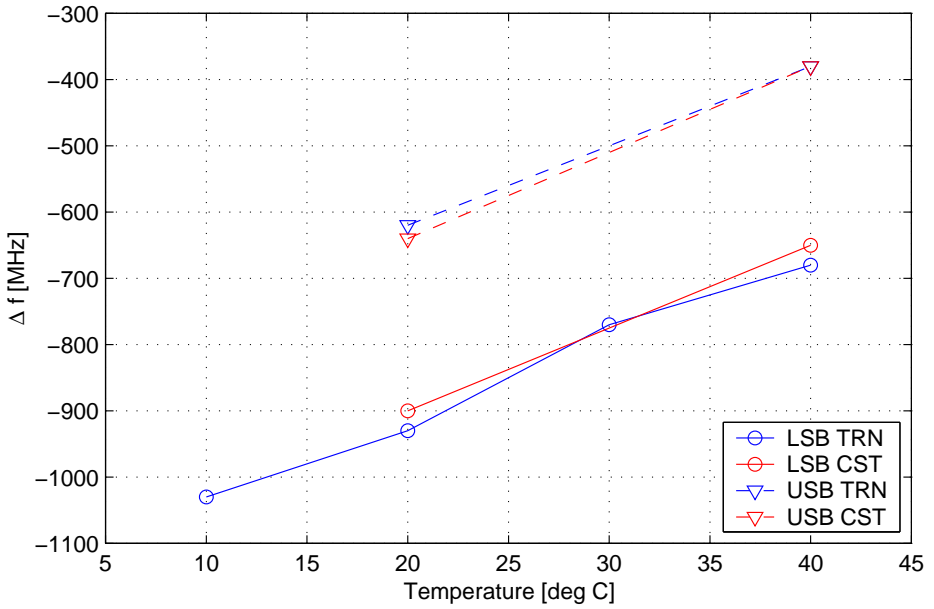


Figure 15: Difference between the measured LSB and USB rejection frequencies from the band centers 625.32 GHz and 649.32 GHz, respectively.

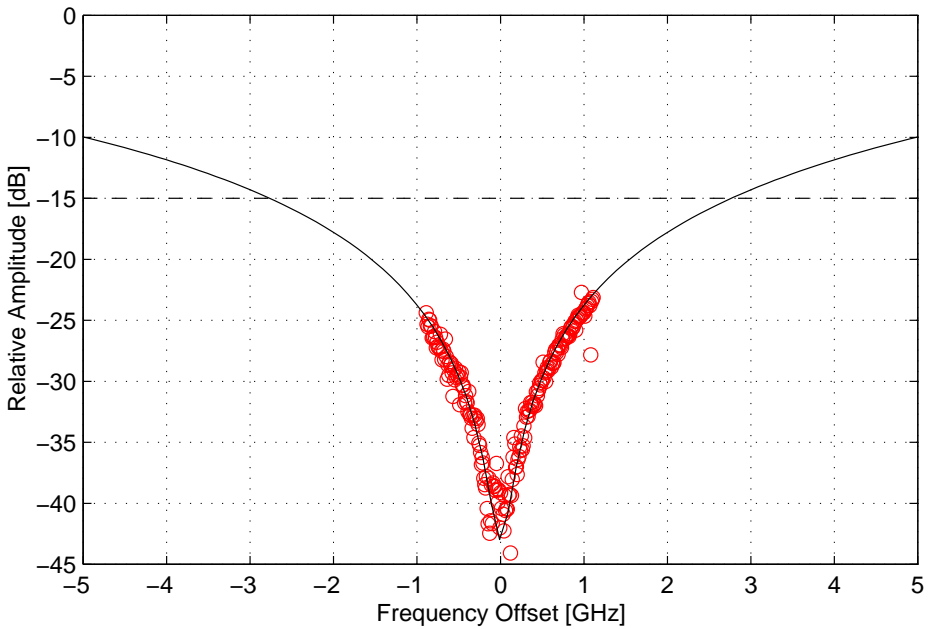


Figure 16: Extrapolation of a bandpass measurement in the LSB. The frequency axis gives the offset from the rejection frequency to demonstrate that the -15 dB level is reached at frequency offsets of about ± 2.8 GHz.

3 SLO Integration

The performance tests of the integrated SLO are twofold. First, it had to be proved that the coupling ratio between the SLO and the COPT is close to the required 5%. Second, it was necessary to verify that the SLO power is distributed equally between the two COPT polarizations. These tests were repeated before and after vibration of the AOPT with integrated SLO and at different temperatures.

3.1 SLO Coupling

A first indication that the SLO coupling ratio would be close to the required 5% are the S11 measurements of the CST path with a metal reflector at the position of the SLO (JEM/SMILES AOPT EM, Part 3: Internal Reflections). From this SLO dummy reflections of about -28 dB were measured, which corresponds to an coupling coefficient of 4%.

The final coupling coefficient of the integrated SLO was determined with a TK absolute power meter. For the SLO alone a total power of $470 \mu W$ was measured before the integration into the AOPT. After integration about $19 \mu W$ were measured at the COPT port, which is already close to the noise of the power meter. This corresponds to a coupling coefficient of 4%. The true SLO coupling ration will be slightly higher than this result because for the measurement at the COPT port only one of the two polarizations can be coupled into the TK power meter head under the Brewster angle.

The TK power meter measures over the whole area of the COPT port. For that reason alignment errors of the SLO signal path would not be detected with this test.

3.2 SLO Balance

The TK power meter is not sensitive enough to measure the SLO balance between the +45 and -45 degrees polarization. For that reason the COPT simulator with the harmonic mixer was used for that test. The IF signal of the mixer had to be observed with a standard spectrum analyzer because a measurement with the ABmm vector receiver would have required some modifications of the SLOC. For this measurement the spectrum analyzer was tuned in zero-span mode to the center frequency of the down-converted SLO signal. Fig. 17 gives an example of such a measurement for the two different polarizations. Typical readings are summarized in the following Tab. 4.

Without the additional cleanup grid in the AOPT the ratio between the two polarizations is worse than -6 dB. Measurements in this configuration before and after vibration did not show any significant changes of that ratio or of the total

	without grid T=22°C	with grid T=22°C	with grid T=40°C
-45°	-31.6 dB	-27.1 dB	-29.5 dB
+45°	-25.2 dB	-27.6 dB	-29.9 dB
SLO balance	-6.4 dB	0.5 dB	0.4 dB

Table 4: Mean values of the spectrum analyzer readings for the two polarizations and resulting SLO balance.

power levels. The large difference of this result from the measurement of the CST path (Fig. 6) can be explained by the fact that in the case of the SLO 95% of the power are cross-polar to RG1, which leads to a much higher contribution of the of the RG1 cross-polar leakage to the detected signal.

With the additional grid the effect of cross-polar leakage is removed. This results in an acceptable SLO balance of 0.5 dB (0.4 dB at 41°C). From these measurements at a fixed frequency alone it is not possible to determine whether the SLO balance will improve or degrade when the AOPT is operated in vacuum. But since these results are consistent with the CST measurements in Fig. 7 it can be expected that the SLO balance will improve under vacuum conditions.

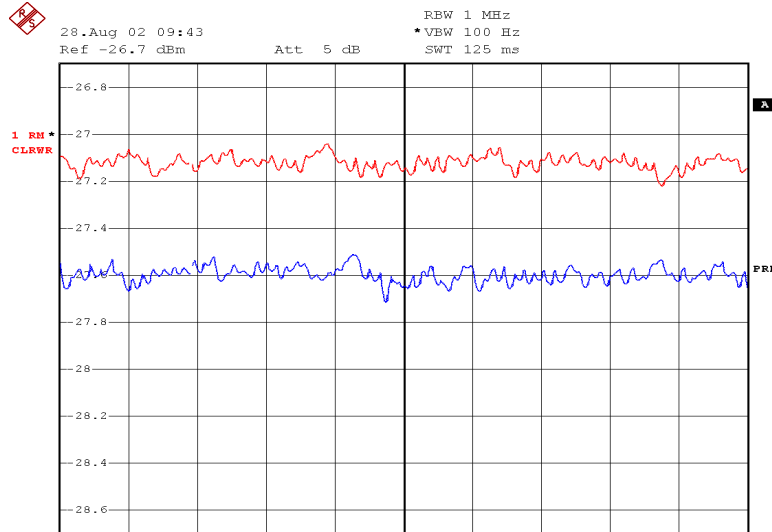


Figure 17: IF signal of the harmonic mixer for -45° (red) and $+45^\circ$ (blue) polarization, analyzed with a spectrum analyzer in zero span mode at 59.22 MHz.

4 Internal Reflections with SMI and SLO

To determine the internal reflections with activated SMI the test procedure had to be slightly modified. For the results in the previous report a reflector at the outside aperture of the TRN BBH was used as reference plane. Since this is no longer possible with the activated SMI the aperture of the CST BBH was used instead. The different lengths of the TRN and CST BBHs is leading to a constant offset of -115 mm on all distances compared to former results. In addition all reflections will be slightly overestimated because of the bias from the 95% coupling coefficient between CST and COPT. The following figures show S11 measurements before SLO integration, where the SLO dummy was replaced by a piece of RAM, as well as measurements with the integrated SLO after vibration.

The effect of the SMI is demonstrated best by the reference measurements in Fig. 18 and 19 where the reflections of a flat aluminum reflector at the TRN aperture is suppressed by -35 dB and -25 dB in the LSB and USB, respectively. The difference between these measurements indicates, however, that the suppression maximum was not located between the two sidebands as designed. After SLO integration and vibration the suppression is almost -30 dB in both sidebands (Fig. 22 and 23).

Before SLO integration the reflections in the CST path alone are mostly caused by the aperture of the CST BBH with amplitudes of about -55 dB (Fig. 20 and 21). After integration of the SLO much higher reflectivities were observed. When the SLO is switched on and its multiplier is properly biased the internal reflections vary between -45 and -33 dB with a periodicity of about 1.2 GHz (Fig. 24 and 25). If standing waves have to be corrected during the retrieval of atmospheric data from SMILES measurements this frequency dependence of the reflections could complicate the procedure. When the 5% coupling efficiency between RG1 and LG1 is taken into account a reflectivity between -17 dB and -5 dB can be calculated for the SLO itself. When the SLO is switched off the matching of the multiplier is worse and the reflections rise by up to 5 dB, in addition to a small phase shift of their periodic ripple.

In the TRN path reflectivities below -60 dB were observed before SLO integration with no FFT signature at the position of the BBH aperture. This is a noticeable improvement from the measurements in the previous S11 report caused by the SMI. Slightly higher reflections of about -55 dB from a distance corresponding to the BBH aperture were detected after SLO integration. They might be caused by a small misalignment of the reflectometer in the COPT simulator. In that context it should be noted that the SMI is less effective if the reflectivity of an aperture or object is polarization dependent. This is presumably the case for the reflections at the BBH aperture in the presence of misalignment. The effect of AOPT/COPT misalignment with the current ICD tolerances (0.5 mm, 0.2°) was

not investigated in detail, but it can be expected that this will lead to a significant increase of the internal reflections.

The diameter of the beam transfer aperture in the COPT simulator was enlarged from 25 to 50 mm, which is similar to the aperture in the AOPT, because previous S11 measurements indicated reflections from the corresponding distance. With this change no more spurious FFT signatures were detected at the position of the COPT aperture.

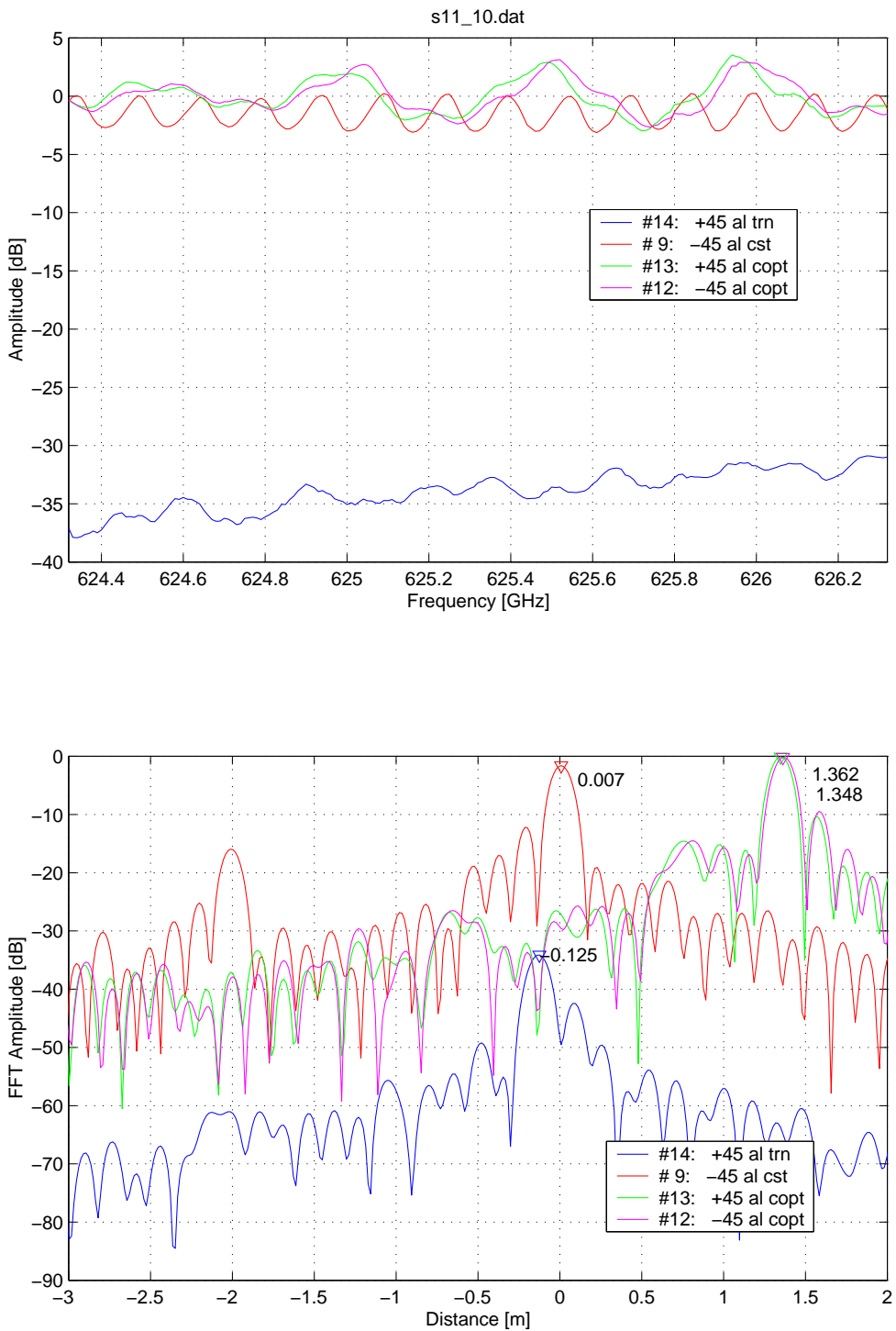


Figure 18: AOPT S11 measurement in the LSB with an Al reflector at one of the BBH apertures or at the COPT port (SMI activated, SLO replaced with RAM).

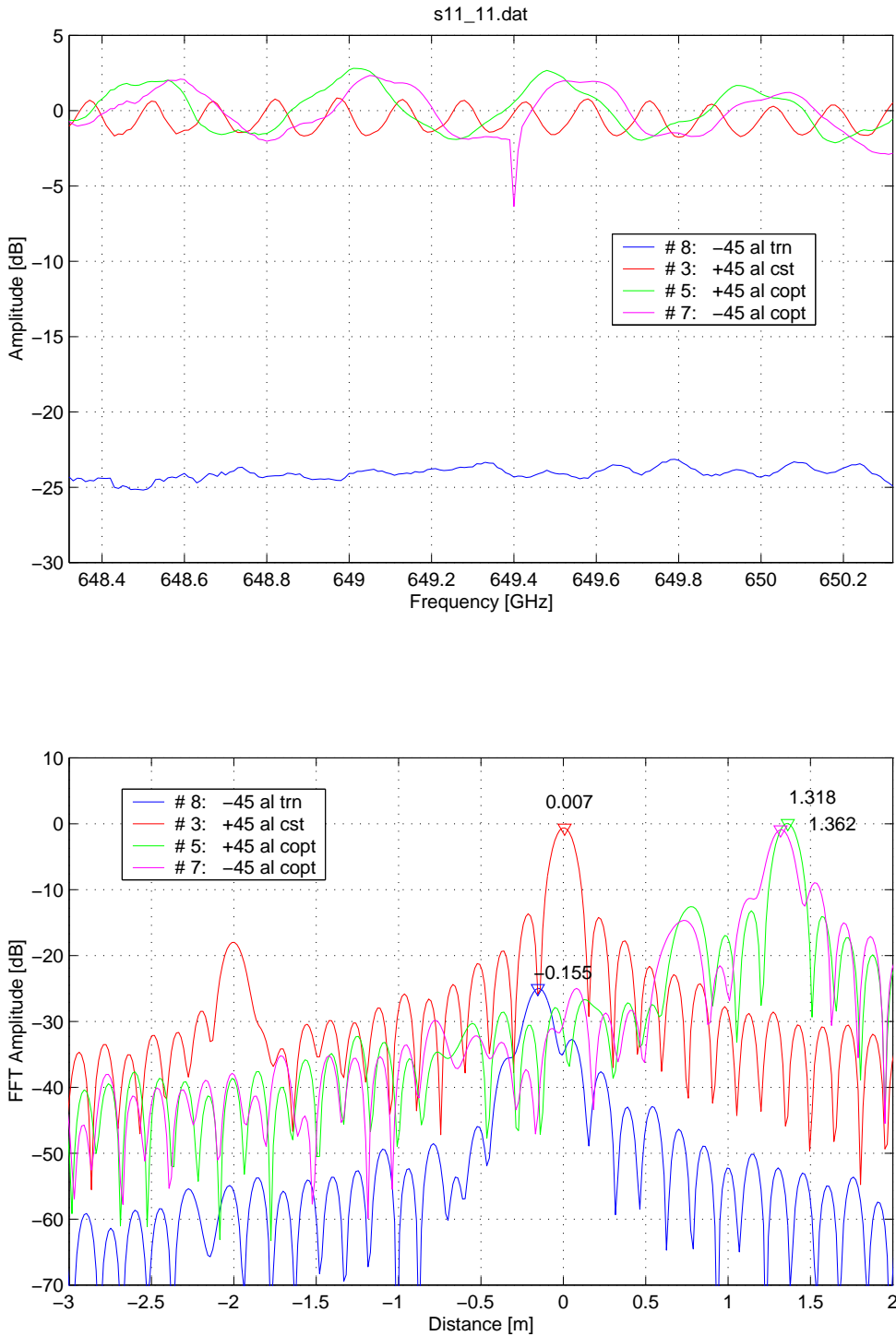


Figure 19: AOPT S11 measurement in the USB with an Al reflector at one of the BBH apertures or at the COPT port (SMI activated, SLO replaced with RAM).

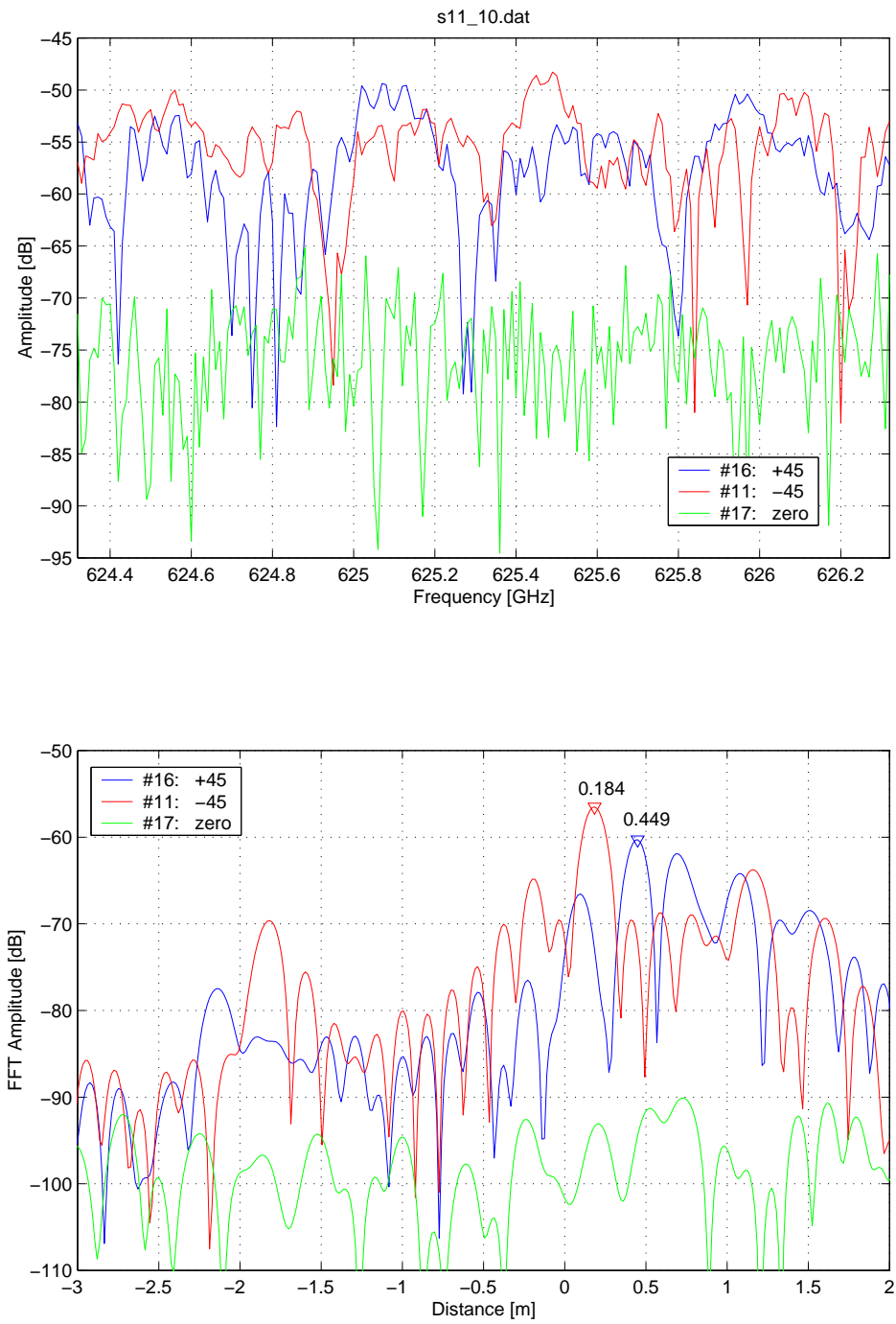


Figure 20: AOPT S11 measurement in the LSB of the TRN (+45) and CST (-45) path together with the noise floor (SMI activated, SLO replaced with RAM).

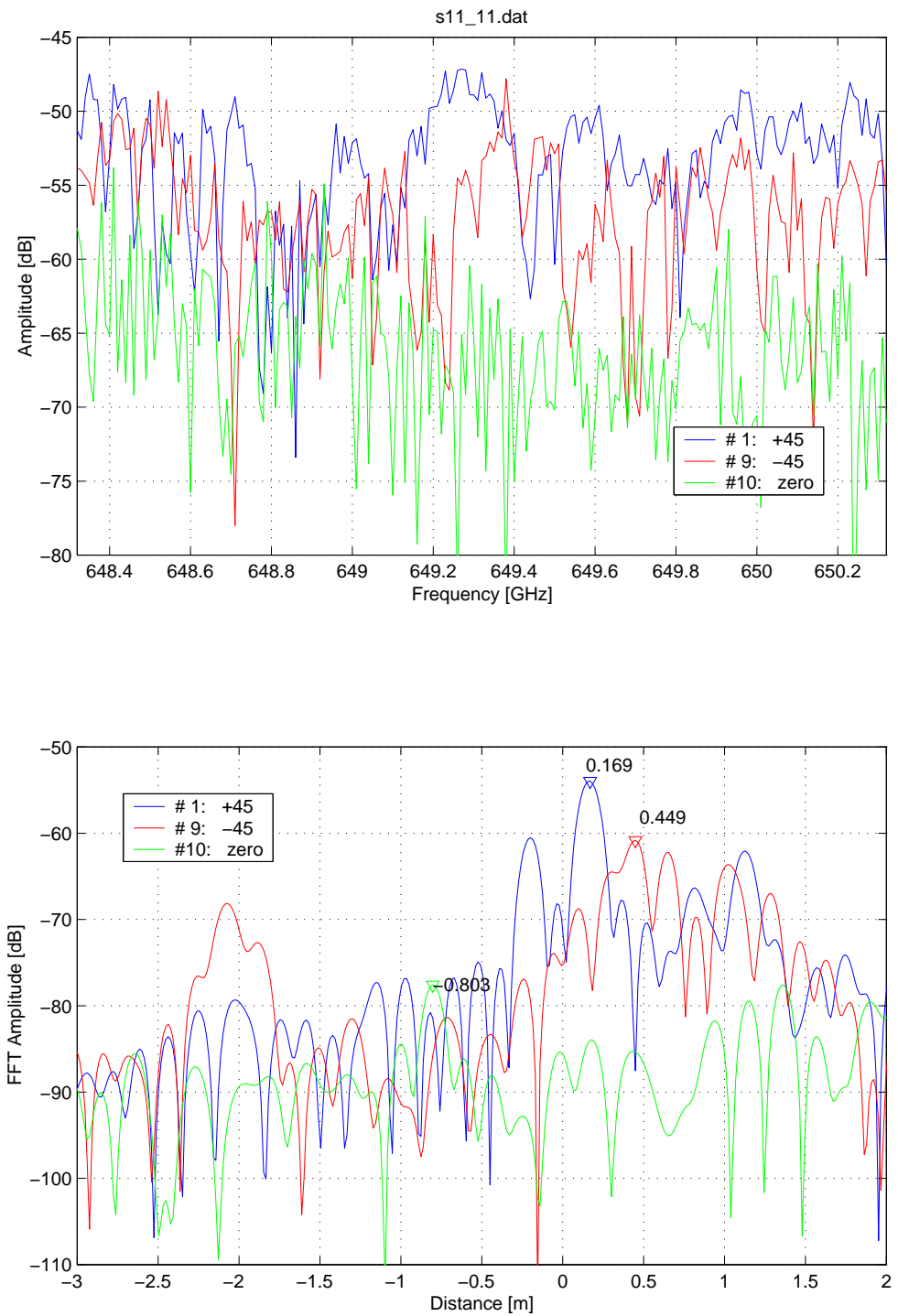


Figure 21: AOPT S11 measurement in the USB of the TRN (-45) and CST (+45) path together with the noise floor (SMI activated, SLO replaced with RAM).

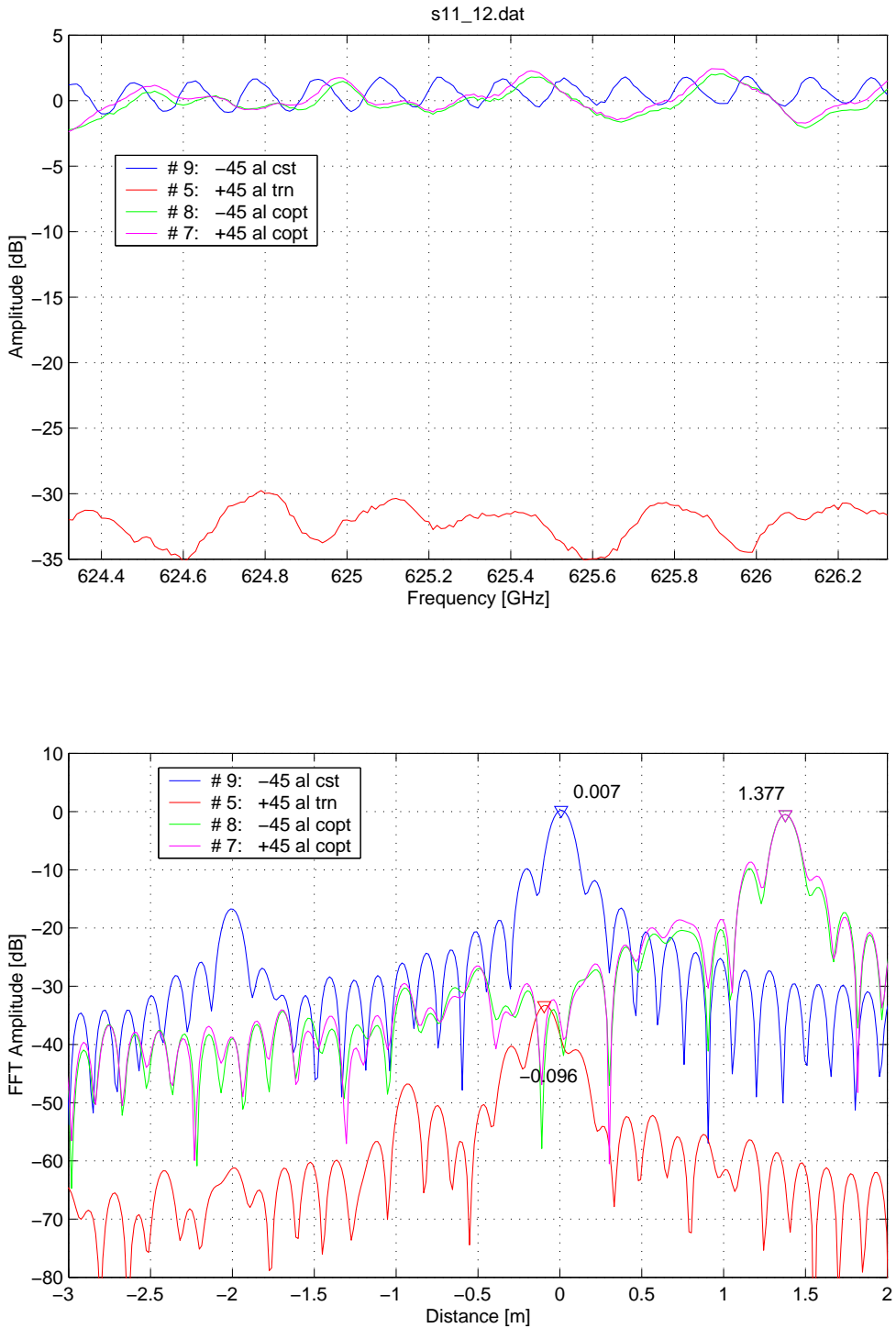


Figure 22: AOPT S11 measurement in the LSB with an Al reflector at the one of BBH apertures or at the COPT port (SMI activated, SLO integrated).

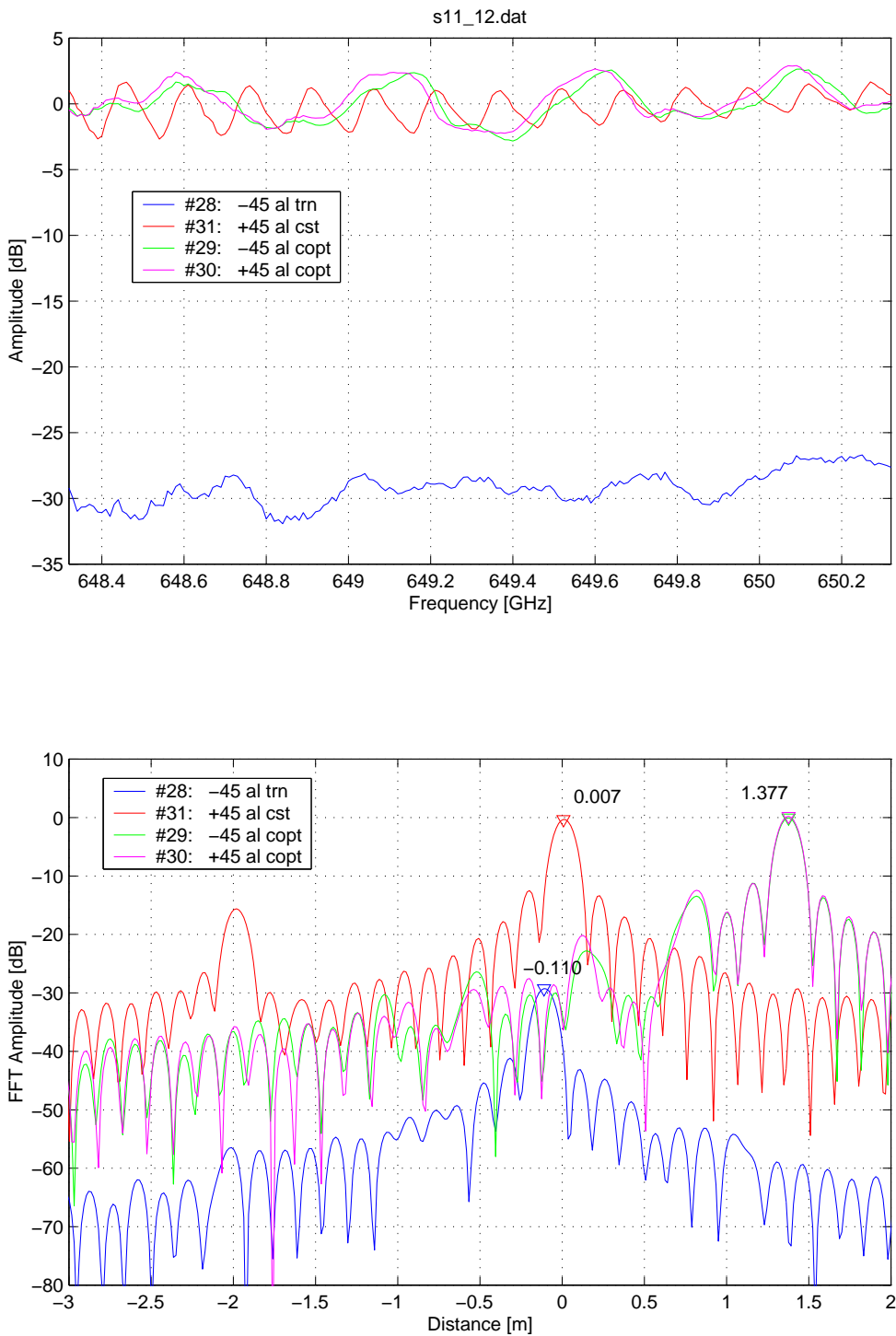


Figure 23: AOPT S11 measurement in the USB with an Al reflector at one of the BBH apertures or at the COPT port (SMI activated, SLO integrated).

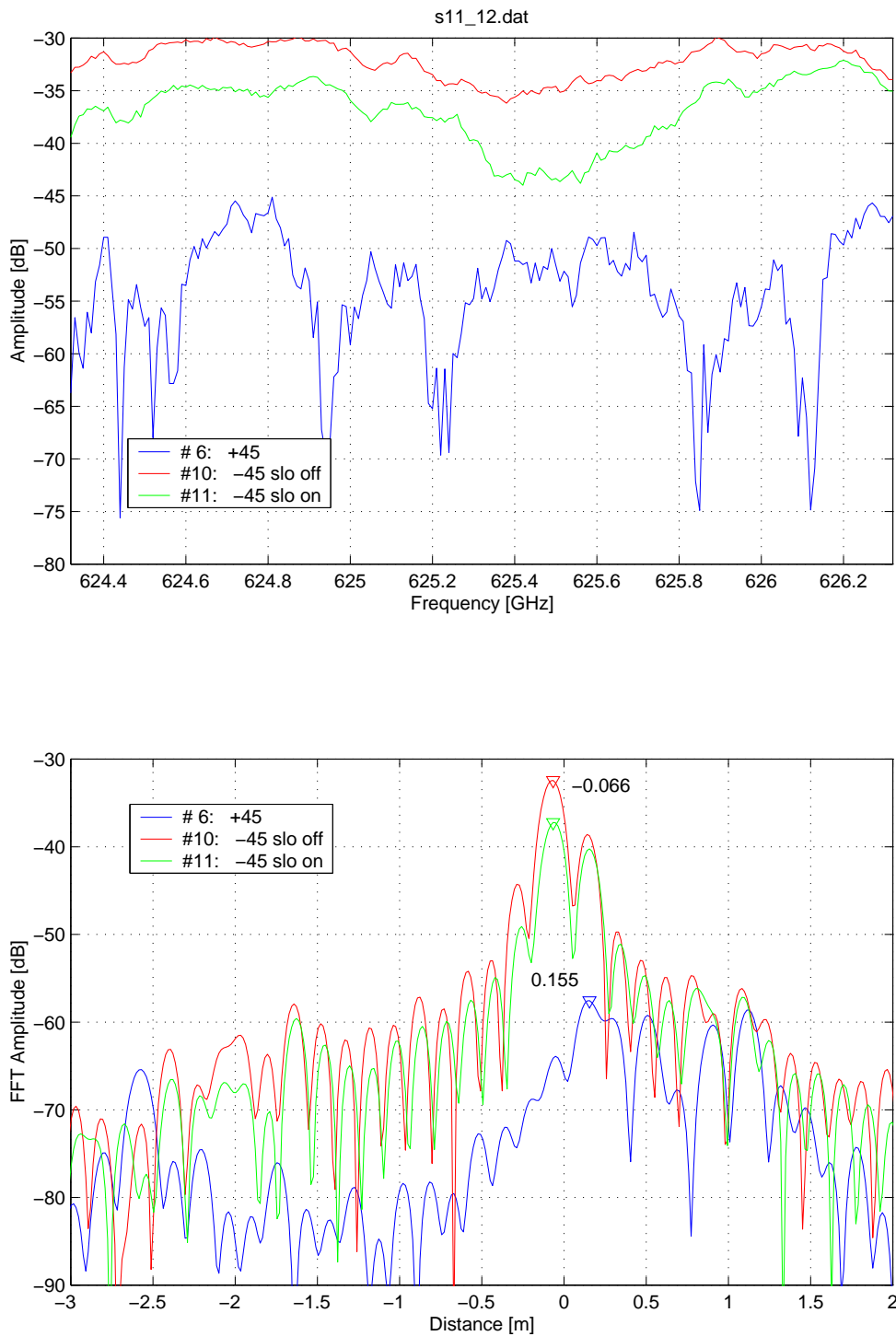


Figure 24: AOPT S11 measurement in the LSB of the TRN (+45) and CST (-45) path together with the noise floor (SMI activated, SLO integrated).

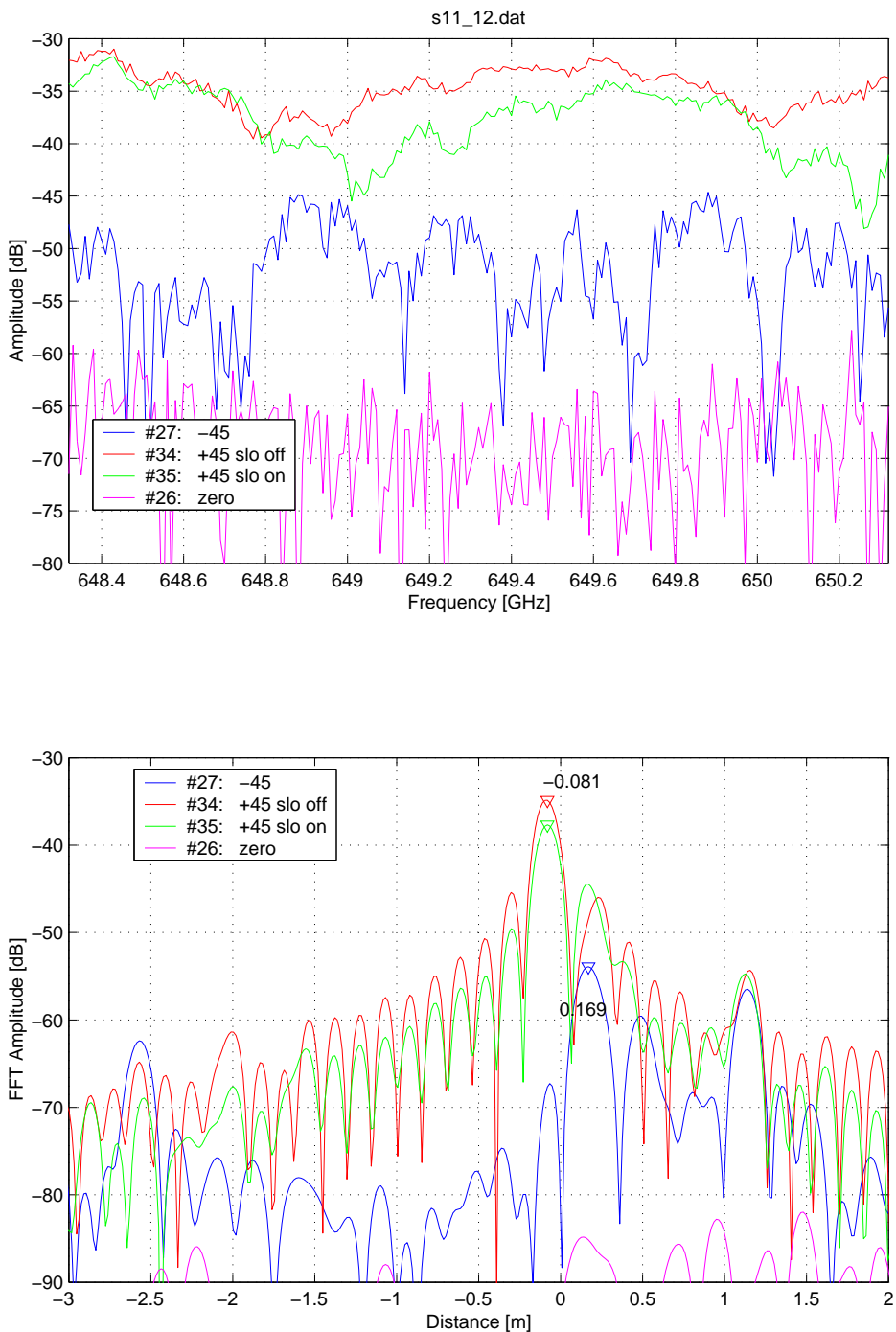


Figure 25: AOPT S11 measurement in the USB of the TRN (-45) and CST (+45) path together with the noise floor (SMI activated, SLO integrated).

5 Conclusions

The measurement in this report have shown that the bandpass characteristic of the FSP sideband filter is not only affected by the cross-polar leakage of the FSP grids, but also of the first polarizing grid RG1 within the AOPT. To avoid these problems the design of the AOPT was changed and includes now an additional cleanup grid in the CST/SLO optical path and a double grid RG1 to improve the polarization purity in the TRN path. With this configuration it was possible to achieve an identical performance of the TRN and CST path which is independent from the input polarization.

Under laboratory conditions the image rejection frequencies were 900 MHz lower than the design value in the LSB, and 600 MHz in the USB. Operation in vacuum will improve this by almost 200 MHz. The FSP sideband filter shows a larger temperature dependence than expected. Part of this frequency shift can be explained by mechanical stress from the different thermal expansions of Aluminum and Invar, but this effect is not fully understood yet. Heating the AOPT to 40°C shifted the characteristic frequencies about +250 MHz closer to the center of the two sidebands. At +10°C the image rejection degraded, but remained still below the -15 dB requirement over the full bandwidth of LSB and USB.

The coupling coefficient of the SLO and its balance between the two polarizations were measured to be close to the specified values. At low AOPT temperatures and in air the SLO balance might become slightly worse than the 0.5 dB requirement, but this should be compensated by the improvement when the air is removed.

The S11 measurements in this report demonstrated that the SMI can reduce reflections in the TRN path by up to -35 dB. After vibration a similar SMI performance was achieved in both sidebands. Very low reflections below -60 dB have been demonstrated for the TRN BBH. The total internal reflections of the AOPT, however, are dominated by the reflections at the SLO in the CST path. These reflections drop by up to -5 dB when the SLO is switched on and its multiplier is properly biased. In this case they vary between -45 and -33 dB with a periodicity of about 1.2 GHz. Together with the 5% coupling efficiency between RG1 and LG1 this indicates a relative poor matching of the SLO itself with values between -17 dB and -5 dB.